Corrosion of carbon steel in artificial soil: Processes occurring during wet/dry transitions studied with a multi-coupon electrode

R. Akkouche, C. Rémazeilles, M. Jeannin, M. Barbalat, Ph. Refait

To cite this version:

R. Akkouche, C. Rémazeilles, M. Jeannin, M. Barbalat, Ph. Refait. Corrosion of carbon steel in artificial soil: Processes occurring during wet/dry transitions studied with a multi-coupon electrode. Electrochimica Acta, 2023, 462, pp.142745. 10.1016/j.electacta.2023.142745 . hal-04692052

HAL Id: hal-04692052
https://hal.science/hal-04692052v1

Submitted on 9 Jul 2025

Electrochimica Acta 462 (2023) 142745

Contents lists available at ScienceDirect

Electrochimica Acta

journal homepage: www.journals.elsevier.com/electrochimica-acta

Corrosion of carbon steel in artificial soil: Processes occurring during wet/dry transitions studied with a multi-coupon electrode

R. Akkouche [a,b], C. Rémazeilles [a,b], M. Jeannin [a], M. Barbalat [b], Ph. Refait [a,*]

[a] Laboratoire des Sciences de l'Ingénieur pour l'Environnement (LaSIE), UMR 7356 CNRS- La Rochelle Université, Bât. Marie Curie, Av. Michel Crépeau cedex 01, La Rochelle F-17042, France
[b] AIR LIQUIDE Research & Development, 1 Chemin de la Porte des Loges, Les Loges en Josas F-78350, France

ARTICLE INFO

Keywords:
Steel
Buried pipelines
Oxygen reduction
Unsatured soil
Differential aeration cell

ABSTRACT

A multi-coupon electrode, composed of 16 square (5 mm × 5 mm) carbon steel coupons, was buried at room temperature during 125 days in an artificial silt loam soil. The soil was initially set at 75% of the saturation with a 0.01 M NaCl + 0.01 M $NaHCO_3$ solution in a specific electrochemical cell. The experimental cell was hermetically closed for 32 days before to be opened so that the effects induced by the progressive drying of the soil could be studied. The OCP and the soil electrolyte resistance R_s, determined by electrochemical impedance spectroscopy, were then monitored over time for each coupon. During the drying process, different behaviors were observed for the various coupons, demonstrating the heterogeneity of this process. XRD analysis of the corrosion product layer covering each coupon at the end of the experiment revealed significant variations of composition from one coupon to another. The composition of the corrosion product layers could be interpreted in link with the OCP and R_s measured values.

1. Introduction

Numerous works, for instance [1–14] among many others, were devoted to corrosion of carbon steel in soil because of its economic significance. Actually, the main method for the transportation of oil, natural gas or drinking water is through buried pipelines. In France, there are for instance 37,000 km of buried pipelines for natural gas only. Besides, many other steel structures are also used underground, in particular in landscape architecture (tubular driven piling, sheet piling…).

Many studies consistently reported that the most influential parameter was soil moisture as it controls the transport of O_2 in the soil [1–9]. In unsaturated soils, water may not be homogeneously distributed so that, with respect to the average soil moisture, wetter and drier zones of soil may coexist. This could be demonstrated via measurements of soil electrolyte resistance R_s using electrochemical impedance spectroscopy (EIS) [5] because R_s increases when the soil at the vicinity of the metal is drying and, conversely, decreases when the soil is wetted [6]. More precisely, in an unsaturated soil, part of the metal surface is in contact with the gas phase and does not participate to the electrochemical reactions. Only the "wet" area of the metal, that is the area in contact with the electrolyte present in the pores of the soil, can be electrochemically active. An increase in R_s actually indicates that the "wet" area has decreased and, conversely, a decrease in R_s would indicate that the "wet" area has increased [5–7].

The heterogeneity of soil moisture can be induced or aggravated during drying or wetting periods [7]. In any case, it gives rise to differential aeration cells and thus induces localized corrosion [6–8]. Cathodic and anodic zones are formed on the steel surface, and electrochemical data, such as corrosion current density j_{corr}, can be correctly interpreted only if the area of the anodic regions is determined, e.g., from post-experiment optical microscopic observations of the corroded surface [8]. The heterogeneous distribution of water may be facilitated in a heterogeneous soil, for instance a soil consisting of a mixture of sand and clay. Soil water retention, a key point controlling the link between soil moisture content and maximal corrosion rate [9], differs strongly for sand and clay, implying that sand-rich areas dry easier and thus faster than clay-rich regions. Sand-rich regions are then characterized by a higher oxygen permeability.

Previous studies focused on galvanic cells formed with a first steel electrode buried in sand coupled to a second steel electrode buried in clay. They showed that significant galvanic effects could indeed take place [10,11]. Such galvanic effects are influenced by wet/dry cycling [11] because soil dynamics are controlled by water retention and thus

---

[*] Corresponding author.
E-mail address: prefait@univ-lr.fr (Ph. Refait).

https://doi.org/10.1016/j.electacta.2023.142745
Received 1 March 2023; Received in revised form 14 June 2023; Accepted 14 June 2023
Available online 15 June 2023
0013-4686/

by the type of soil (i.e., sand, silk or clay). A galvanic cell was also designed with carbon steel coupons buried in the same soil in two regions, separated with an ion-exchange membrane, characterized by different soil moistures [12]. The authors used a so-called “many-electrode glass cell” to observe the behavior of steel with respect to the distance from the wet soil/dry soil interface. This study also evidenced significant effects. Other authors developed a similar approach based on a multi-electrode system, such as the wire-beam electrode (WBE) [13,14]. The WBE is an assembly of ~100 mild steel wires with a diameter of 1.5 mm, embedded in epoxy resin so that they are insulated from each other with a very thin layer of resin. This assembly forms a (approximately) 15 mm × 15 mm square electrode [13]. A map of anodic and cathodic areas can then be obtained and a monitoring of the behavior of each mild steel beam allows observing the initiation, propagation and/or disappearance of these areas [13].

The corrosion product layer forming on the steel surface may play a major role on the evolution of the galvanic effects associated with differential aeration. It may hinder or favor the persistence of these effects depending on the nature of the corrosion products that form on the steel surface in anodic and cathodic zones. If the corrosion products forming on cathodic zones of the steel surface are insulators, they may hinder, via a barrier effect, the transport of oxygen towards the metal surface and thus progressively reduce the impact of differential aeration. In contrast, if electronic conductors such as magnetite (Fe_3O_4) are favored in the cathodic zones, they may facilitate O_2 reduction. In this case, O_2 does not need to reach the steel surface as it can be reduced on the outer surface of the corrosion product layer. In this case, the galvanic effect due to differential aeration can persist for longer times, as shown for carbon steel immersed in seawater [15,16].

The present study is the first one, to our better knowledge, to address the possible link between differential aeration cells created during soil natural changes (i.e., drying or wetting) and composition of corrosion product layer. For that purpose, a specific multi-coupon electrode (MCE) was designed and used for the first time with the aim to combine, for each individual coupon of the MCE, in situ electrochemical measurements and ex situ X-Ray diffraction (XRD) analysis of the corrosion products. The MCE consisted of 16 square steel coupons (5 mm × 5 mm) with an individual electric connection to achieve electrochemical measurements on each coupon. A large active area of 25 mm^2 was considered for the coupons so that the corrosion product layer covering each of them could be characterized by XRD. The number of coupons, i.e., 16, was chosen to give a 400 mm^2 large surface of metal in contact with the soil, assumed to be sufficient to point out corrosion phenomena associated with the heterogeneity of the soil during drying and wetting stages. The evolution of open circuit potential (OCP) and R_s (determined by EIS) was monitored over time for each coupon and for the whole MCE. The OCP of a coupon would be indicative of the local aeration level of the soil, increasing with increasing O_2 content [6–8], while its R_s would be indicative of the local moisture level, decreasing with increasing water content [5–7]. Consequently, a (qualitative) mapping of soil moisture at the vicinity of the steel surface, and its evolution with time during soil dynamics (i.e., drying and wetting), is obtained here for the first time.

The artificial silt loam soil used for this study was initially wetted at 75% of the saturation level (75% sat.) using a $NaHCO_3 + NaCl$ solution. After 31 days, the soil was dried slowly. It was rewetted at day 115 and the experiment was stopped 10 days later, for an overall duration of ~4 months. The MCE was then extracted from the soil and the corrosion product layer covering each of the 16 coupons of the MCE was characterized by XRD. Finally, the surface of each coupon was studied by optical microscopy (OM) after removal of the corrosion products. The morphology of the degradation, the size and the depth of the various localized corroded zones could then be determined for each coupon. Localized corrosion rates were estimated thanks to these OM measurements. The link between corrosion processes, corrosion product layer, and evolution of measured electrochemical parameters during drying of the soil is thoroughly discussed.

2. Materials and methods

2.1. Materials

The S235JR carbon steel commonly used for pipelines was considered for the present study. The average composition of the material used (in weight%) was: 0.097% C, 0.49% Mn, 0.020% P, 0.09% Si, 0.05% Cr, 0.11% Ni, 0.16% Cu, 0.042% S and Fe for the rest. All the steel coupons were prepared from the same portion of a 1-meter diameter tube.

The multi-coupon electrode (MCE) was composed of 16 coupons, each one having an active area of 5 mm × 5 mm and a thickness of 4 mm. The distance between each coupon was set at 1 mm. It was assumed to be sufficiently small so that the whole MCE behaves as a homogeneous electrode. A copper wire was welded on one side of each coupon while the four lateral sides were varnished. The coupons were finally placed into a 3D-printed mold and embedded in epoxy resin. A schematic representation of the MCE is displayed in Fig. 1, with the matrix indexation chosen to designate each coupon. The MCE was polished with silicon carbide grade 180 (particle size 76 μm) to simulate a shot-blasted surface, rinsed thoroughly with Milli-Q water and rapidly dried in an air flow. The active area of each coupon is 25 mm^2 so that the overall active area of the MCE is equal to 4 cm^2.

The artificial soil considered for the present study was already used in previous work [6]. It was composed of 83 wt.% of fine sand (SiO_2, average particle size 22 μm), 14.5 wt.% of kaolinite, and 2.5 wt.% of peat, which is composed of partially decayed vegetation and organic matter. Therefore, 75% of the soil mass corresponded to mineral particles with a diameter between 2 μm and 50 μm and 20% to particles smaller than 2 μm. This soil can then be classified as a silt loam soil [17]. It was wetted with a 0.01 mol L^{-1} NaCl and 0.01 mol L^{-1} $NaHCO_3$ solution prepared with 98% min. purity NaCl, 99% min. purity $NaHCO_3$ and de-ionized water (resistivity 18.2 MΩ cm). The saturation level (i.e., 100% sat.) of the soil was first determined experimentally by adding progressively the electrolyte to a definite mass of dried soil in a beaker until water accumulated on top of the wetted soil surface. Then the amount of water to be added to the dried soil to reach the saturation level considered for the experiment could be computed. For the current study, the soil was prepared with an initial moisture content corresponding to 75% sat. The resulting pH of the soil, measured at the beginning of the experiment, was 7.3 ± 0.1.

The experiment was carried out at room temperature, i.e., 21±2 °C during the corresponding period of the year.

2.2. Electrochemical measurements and wet/dry cycling

A schematic view of the electrochemical cell used for the present study is presented in Fig. 2. The cylindrical cell, 25 cm high and 20 cm in

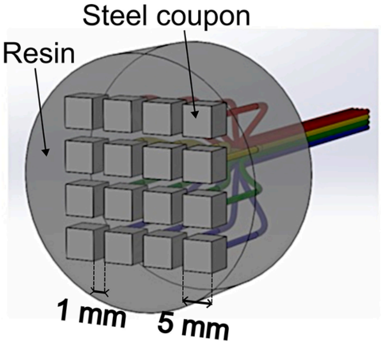

11	12	13	14
21	22	23	24
31	32	33	34
41	42	43	44

Fig. 1. Schematic representation of the multi-coupon electrode and the matrix numbering used to identify the coupons.

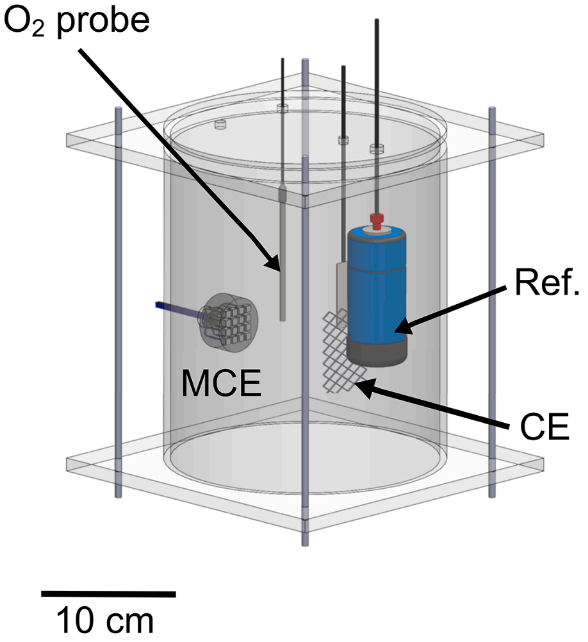

Fig. 2. Schematic representation of the electrochemical cell designed for the study of the corrosion of carbon steel buried in soil.

diameter, was made in Plexiglas. The upper lid was initially sealed to maintain a constant moisture in the soil. The reference electrode (blue cylinder in Fig. 2) was a copper-copper sulfate electrode (CSE, +0.316 V/SHE at 25 °C) designed for measurements in soil (Corexco CELCO 5) and the counter electrode was a Pt-coated titanium grid. Oxygen content was measured using a PSt3 oxygen sensor buried in the soil all along the experiment. It was connected to a Fibox 4 fiber optic oxygen transmitter (PreSens). The PSt3 sensor has a detection threshold of 0.03% (gas) or 15 ppb (dissolved) oxygen. The oxygen content in the soil ($[O_2]$) was measured each 30 min.

The MCE and the oxygen probe were set at the same depth on a semi-circle that faced the reference and counter electrodes. They were buried under 10 cm of soil and the cell was not entirely filled with soil, a thick layer (~5 cm) of air being left to constitute a reservoir of oxygen to fuel the corrosion process when the cell was sealed. A slow drying of the soil was achieved at day 32 by simply removing the lid and exposing the soil to the atmosphere during 2 h. The lid was set back afterwards, the cell sealed again. This procedure proved sufficient to induce a partial drying of the top of the soil, which was followed by an evolution of the overall soil system. This evolution of the soil led to a progressive and slow evolution of the MCE/soil interface. The soil was sightly rewetted at day 74 before the cell was opened again at day 75 for a further drying of the soil. At day 115, the soil was re-wetted by addition of de-ionized water and the cell closed once more. The experiment was finally stopped at day 125.

The behavior of each coupon was followed over time via the monitoring of two parameters, the open circuit potential (OCP) and the soil electrolyte resistance R_s, determined by EIS. All measurements were carried out with a Gamry1000 potentiostat. For EIS measurements, devoted to the determination of the soil electrolyte resistance, only the high frequency range was investigated, from 100 kHz to 100 Hz, with ten points per decade. The AC voltage perturbation amplitude (peak to peak) was set at 30 mV because of the important ohmic drop characteristic of unsaturated soils. The linearity of the system was checked in varying the amplitude of the AC signal. R_s was determined directly from the Nyquist representation of the EIS data, i.e., without any modeling via an equivalent electrical circuit. The accuracy of an OCP measurement was determined to be equal to ±2 mV, independently of the measured OCP value, while that of R_s was ±5%.

Note finally that a soil moisture sensor (Waterscout SM100 sensor - Spectrum Technologies) was buried in the cell as for previous study [6]. The corresponding data, that gave information about the evolution of soil moisture at the vicinity of the sensor, were not considered because they were not exactly representative (even if they were somewhat similar) of the evolution of soil humidity at the vicinity of the MCE. Consequently, this sensor was omitted in Fig. 2. The results described and discussed in the following actually confirm how the drying process can be heterogeneous so that only a local information is relevant [7].

2.3. Characterization of the coupons surface

At the end of the experiment, the MCE was removed from the cell. It was covered with a 2–3 mm thick layer of soil that adhered to the underlying corrosion product layer. This remaining soil was carefully scraped on each coupon until a change of color indicated the presence of rust. The corrosion product layer was then characterized by X-ray diffraction (XRD). A drop of glycerol was poured on the surface of the coupons so that the pores of the corrosion product layers were impregnated with glycerol, thus preventing the oxidation by air of Fe(II)-based corrosion products [18]. The XRD analysis was carried out with an Inel EQUINOX 6000 diffractometer using Co-Kα radiation ($\lambda = 0.17903$ nm). The diffractometer was equipped with a CPS 590 curved detector designed for the simultaneous detection of the diffracted photons on a 2θ range of 90° The XRD pattern was obtained in any case with a constant angle of incidence (5°) and an acquisition time of 45 min.

The X-ray beam was focused to limit the analysis to a square area of 4 mm × 4 mm. Each coupon (with a surface of 5 mm × 5 mm) composing the MCE was placed in turn under the beam. In some cases, the first XRD analysis only revealed the presence of components of the soil. Another part of the mineral layer was then scraped from the surface and the coupon was analyzed once more. The various phases were identified via the ICDD-JCPDS database. The files used for the various compounds were 01–078–2110 (kaolinite), 01–086–1560 (quartz), 00–040–0127 (chloride green rust), 01–074–3400 (sulfate green rust), 00–050–1380 (carbonate green rust), 00–029–0713 (goethite), 00–044–1415 (lepidocrocite), 01–082–1533 (magnetite) and 00–029–0696 (siderite). The angular scale was calibrated using the diffraction lines of a-Fe present in each case and characteristic of the steel substrate.

Once thoroughly characterized, the corrosion product layer was removed from the MCE surface according to the NF-ISO 8407:2010 standard [19], i.e., using a solution of hydrochloric acid (HCl) and hexamethylenetetramine. Images of the coupons surface, corrosion depth profiles and quantification of local corrosion damages were obtained using a LEICA DM 6000 M optical microscope (OM).

3. Experimental results

3.1. Evolution of OCP and O_2 content

Fig. 3 displays the evolution of $[O_2]$ and OCP (of whole MCE), during the 125 days of experiment. The gaps in OCP measurements correspond to periods where measurements were interrupted, sometimes involuntarily. The dotted vertical lines point out the moments when the cell was opened, closed or when water was added. The evolution of both OCP and $[O_2]$ over time clearly reveals these changes. At the beginning, the cell was hermetically sealed, the soil was initially very wet (75% sat.). $[O_2]$ decreased rapidly during the first days due to the consumption of O_2 by steel corrosion processes, and reached the detection threshold of the probe. It can be noted that the first OCP value, measured 3 h after closing the cell, was already low, as low as the values measured when $[O_2]$ finally reached the detection threshold. It is likely that the O_2 molecules initially present at the vicinity of the steel surface were already consumed after 3 h, leading to this low OCP value. In contrast, the O_2 probe was not buried at the immediate vicinity of the MCE so that the decrease in O_2 concentration in the soil around the probe was delayed.

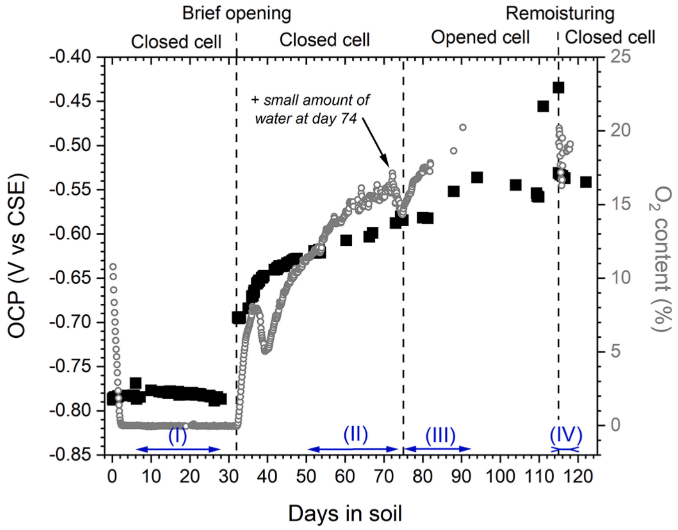

Fig. 3. Evolution of the OCP of the whole MCE and O_2 content of the soil during the experiment. The blue arrows (I) to (IV) indicate the 4 considered time periods (see text, Section 3.2).

On day 32, the cell was opened for 2 h, which led to a significant change so that [O_2] increased sharply up to 8% into four days. It is assumed that this brief opening led to a partial drying of the soil and then favoured the transport of O_2 as a gas phase in the pores. Consistently, the OCP increased from −0.79 V vs CSE to −0.67 V vs CSE, but varied before any increase in [O_2] was detected by the O_2 probe. It can be forwarded that air reached the MCE before it could reach the [O_2] probe. It is also noticeable that both OCP and [O_2] went on to increase long after the cell was closed again. The hypothesis that can be forwarded is that the upper part of the soil dried when the cell was briefly opened and that the generated gradient of water content subsequently induced (after the cell was closed) a movement of water by capillarity from bottom to top, thus progressively decreasing the water content in lower pores of the soil and thus progressively facilitating the transport of O_2 toward the MCE. It is also possible that large and long cracks were generated in the upper part of the soil, therefore facilitating the transport of air, present at the top of the cell, deeper in the soil.

Between day 37 and day 40, [O_2] decreased, probably because of the resumption of the corrosion process. It increased again afterwards, more slowly, reaching 18% at day 74. The lid of the cell was removed at that time because electrochemical measurements proved difficult, with too much noise on EIS data, and a small amount of water was then added. This amount corresponded approximately to 10% of the volume of water required to remoisturise completely the soil to 75% sat. This operation led to the small decrease in [O_2] observed from day 74 to day 75, which indicated that the moisture content at the vicinity of the O_2 probe had increased.

The cell was opened at day 75 and the soil was left drying. As a result, [O_2] increased again, reaching in this case 20%, i.e., the oxygen content of air, at day 90. The OCP also increased and reached its maximum at the end this period, i.e., −0.434 V vs CSE at day 115. The soil was wetted again at day 115, with a large amount of water to reach the initial conditions. The cell was then sealed for the rest of the experiment (day 125). This water addition had few effects on [O_2] and OCP, which both remained high (18±2% and –0.536±0.005 V vs CSE, respectively).

3.2. *Electrochemical study of the corrosion process of the MCE coupons*

In order to synthetize the electrochemical results obtained with the MCE, four characteristic time periods were considered (see Fig. 3). Period (I) is from day 5 to day 28, when the oxygen concentration is very low, consumed by corrosion processes. After the brief opening of the cell, transient phenomena occurred and the system was rather unstable. This period was then discarded and the considered period (II) goes from day 50 to day 74, when soil moisture and oxygen concentration are increasing slowly. Period (III) corresponds to days 75–92 when the soil is very dry. The final shorter period (IV) follows the re-wetting of the soil at day 115 and corresponds to days 115–118.

The average values of the OCP for each of the 16 coupons of the MCE, computed for the four considered periods, are given in Table 1, with corresponding standard deviations. Moreover, Fig. 4 shows the evolution of the OCP for eight selected coupons.

During period (I), all the coupons have similar OCP values, in the range between −0.79 and −0.77 V vs CSE, which means that the environment is homogeneous at that time. For period (II), an important scattering of OCP values is observed. The OCP varies from −0.73 vs CSE for coupon C33 to −0.43 V vs CSE for coupon C31. This difference in OCP values indicates that the drying of the soil and the resulting increase in [O_2] is a heterogeneous process that leads, during the transient period from wet soil to dry soil, to the coexistence of wet zones of soil and drier zones of soil. Close to the coupons with low OCP values (e.g., C33 and C11), the soil remained rather wet, and thus weakly aerated, while close to the coupons with high OCP values (e.g., C31), the soil was drier and thus more aerated. It must be noted that the overall surface of the O_2 probe is much larger than the surface of one single coupon of the MCE, so that the information given by the probe may be representative of the average aeration level inside the soil at the vicinity of the probe.

A scattering of OCP values is also observed in period (III). The average OCP values are however higher, i.e., range between −0.67 V vs CSE (C32) to −0.37 V vs CSE (C31). In period (III), the soil is on average drier than in period (II), and thus more aerated. In period (IV), after adding water, the scattering of OCP values persisted. For some coupons, the OCP decreased after the addition of water (e.g., C41), which is

Table 1
Average OCP values of the 16 coupons of the MCE over the four periods, in V vs CSE. Periods: (I) = days 5–28; (II) = days 50–74; (III) = days 75–92; (IV) = days 115–118.

Cell state	Closed	*Re*-closed after 1 h opening at day 32	Opened	*Re*-wetted and closed
Period	(I)	(II)	(III)	(IV)
C11	−0.790 ± 0.005	−0.675 ± 0.01	−0.60 ± 0.03	−0.620 ± 0.002
C12	−0.790 ± 0.007	−0.615 ± 0.005	−0.54 ± 0.02	−0.480 ± 0.001
C13	−0.785 ± 0.005	−0.62 ± 0.02	−0.54 ± 0.04	−0.470 ± 0.004
C14	−0.785 ± 0.005	−0.57 ± 0.01	−0.500 ± 0.005	−0.473 ± 0.001
C21	−0.780 ± 0.004	−0.62 ± 0.01	−0.57 ± 0.05	−0.560 ± 0.002
C22	−0.782 ± 0.002	−0.67 ± 0.01	−0.51 ± 0.03	−0.410 ± 0.004
C23	−0.780 ± 0.003	−0.55 ± 0.05	−0.47 ± 0.02	−0.38 ± 0.002
C24	−0.781 ± 0.002	−0.64 ± 0.01	−0.52 ± 0.04	−0.450 ± 0.001
C31	−0.772 ± 0.002	−0.430 ± 0.005	−0.37 ± 0.02	−0.410 ± 0.003
C32	−0.780 ± 0.004	−0.663 ± 0.001	−0.63 ± 0.01	−0.550 ± 0.001
C33	−0.781 ± 0.002	−0.73 ± 0.1	−0.55 ± 0.02	−0.599 ± 0.002
C34	−0.774 ± 0.001	−0.59 ± 0.03	−0.46 ± 0.01	−0.38 ± 0.01
C41	−0.773 ± 0.002	−0.51 ± 0.02	−0.48 ± 0.02	−0.578 ± 0.002
C42	−0.782 ± 0.002	−0.60 ± 0.01	−0.530 ± 0.005	−0.62 ± 0.002
C43	−0.783 ± 0.003	−0.57 ± 0.01	−0.49 ± 0.02	−0.483 ± 0.003
C44	−0.781 ± 0.002	−0.56 ± 0.02	−0.52 ± 0.01	−0.586 ± 0.002

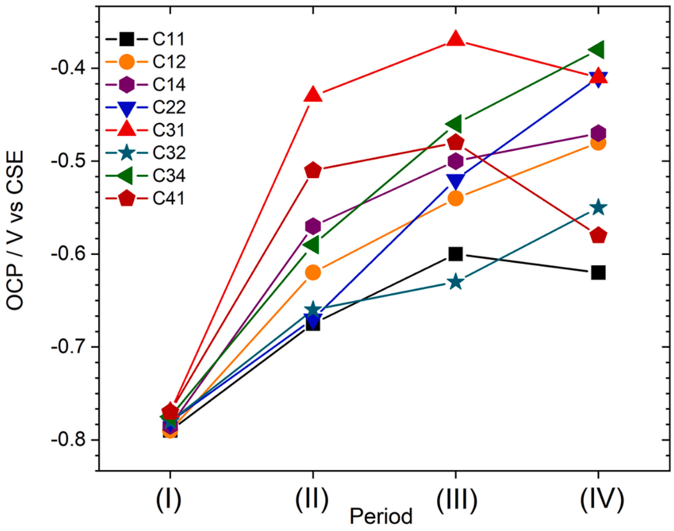

Fig. 4. Evolution of the average OCP values of coupons C11, C12, C14, C22, C31, C32, C34 and C41 over the four considered periods.

consistent with a decreasing aeration level. However, the OCP still increased for other coupons (e.g., C22).

The standard deviations given in Table 1 for each individual coupon also illustrate the various behaviors of the coupons. In any case, standard deviations are very small during period (I) when soil moisture is constant. They are also small in period (IV) but in this short time period only 2–3 measurements were performed for each coupon. In periods (II) and (III), where moisture and aeration varied, the standard deviations are larger as the soil/coupon interface still changes. The small standard deviation for coupon C14 (±5 mV) during period (III) shows that this coupon reached a steady state earlier, and its OCP was stable. In contrast, the large standard deviation for coupon C33 (±100 mV) during period (II) shows that the soil in contact with this coupon had not dried before but was actively drying during period (II). In fact, the OCP of C33 increased from −0.73 V/CSE to −0.53 V/CSE in this period.

To illustrate the spatial distribution of OCP values, a 2D representation of the MCE is displayed in Fig. 5. It relates to average OCP values of period (III) for each coupon. The coupons with low OCP values are depicted as dark squares while the coupons with high OCP values are in light shades. The displayed pattern does not reveal any clear trend. It can even be observed that coupon C31, which has the highest OCP, is adjacent to coupon C32, which is one of the coupons characterized by a very low OCP. More precisely, the difference between the OCP values of coupons C31 and C32 is 0.27 V for period (III), as calculated from Table 1. As those coupons are close to each other, this large difference between the two potentials could be indicative of galvanic effects.

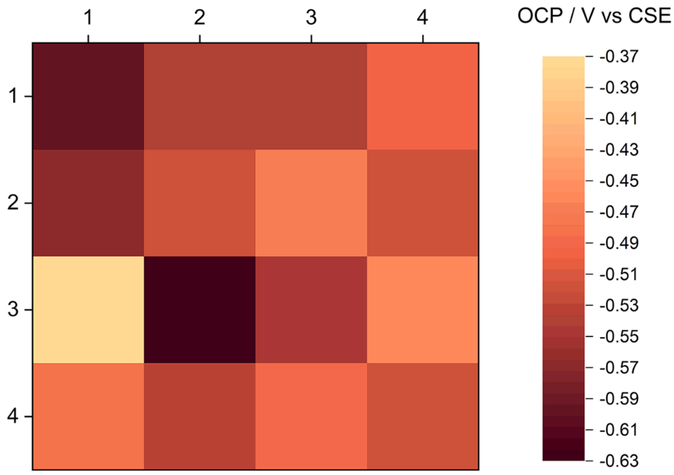

Fig. 5. 2D representation of the average OCP values measured at period (III) for the 16 coupons of the MCE.

A further understanding of corrosion phenomena is given by the variations of soil resistance R_s measured by EIS for each coupon of the MCE. Table 2 gathers the average R_s values for the four considered periods while Fig. 6 illustrates the evolution of R_s for 8 selected coupons (as done for OCP – see Fig. 4).

As for OCP, the R_s values measured in period (I) are quite similar, which means the same soil moisture at the vicinity of each coupon of the MCE. When the soil starts to dry and becomes more aerated, i.e., in periods (II) and (III), an important scattering of R_s values is observed. This result confirms the heterogeneous nature of the soil during its drying.

It can be noted that coupons C11 and C32, that have the lowest OCP values, have also the lowest R_s values. On the other hand, coupons C23 and C34, characterized by a high R_s value, have also a high OCP. Actually, if R_s remains low, the “wet” area of the coupon remains high, which indicates that the soil close to the coupon surface remains rather wet, thus weakly aerated. Therefore, the OCP value should be low. In contrast, a rapid and important increase in R_s corresponds to a rapid and important decrease in the “wet” area. The soil becomes much more aerated and the OCP should be high.

C31 is a particular case. It is characterized by a high OCP value that is associated with a moderate R_s value in periods (II) and (III), indicating that the “wet” area remained important. The high OCP value of C31 could then indicate that the cathodic reaction, i.e., oxygen reduction, was particularly active at the surface of this coupon. This suggests that coupon C31 is acting like a cathode, more likely in connection with coupon C32, which is close to coupon C31 and characterized by a much lower OCP value (and a rather low R_s value indicative of a locally rather wet soil). Another explanation could be an important gradient of chemical composition in the soil around C31.

The 2D representation of R_s values in period (III) is displayed in Fig. 7 and gives a clear view of the dry and wet zones. Four coupons are noticeable: C11 and C32 have the lowest R_s values and thus remained in a rather wet environment. In contrast, C23 and C34 have the highest R_s values and thus were set in a rather dry part of the soil.

Finally, the adding of water at the beginning of period (IV) reduced the scattering of R_s values. This indicates that soil wetness became less heterogeneous. This evolution towards an increased homogeneity was not suggested at all by the evolution of OCP values. Considering that period IV is very short (4 days), it can be considered that OCP values

Table 2
Average R_s values of the 16 coupons of the MCE over the four periods, in Ω cm^2. Periods: (I) = days 5–28; (II) = days 50–75; (III) = days 75–92; (IV) = days 115–118.

Cell state Period	Closed (I)	*Re*-closed after 1 h opening at day 32 (II)	Opened (III)	*Re*-wetted and closed (IV)
C11	600	1200	2000	1000
C12	670	3700	4300	1100
C13	780	4200	5800	1800
C14	610	3400	4100	1500
C21	800	3800	5300	1000
C22	1000	3000	7800	900
C23	2600	30,000	18,000	2000
C24	460	6400	8000	1600
C31	730	2000	6800	2700
C32	650	2100	2800	1200
C33	n.d.	4400	5700	n.d
C34	1700	19,000	25,000	1800
C41	1200	3400	5300	1400
C42	800	2650	5300	1100
C43	1300	6600	7500	3800
C44	820	3500	6000	830

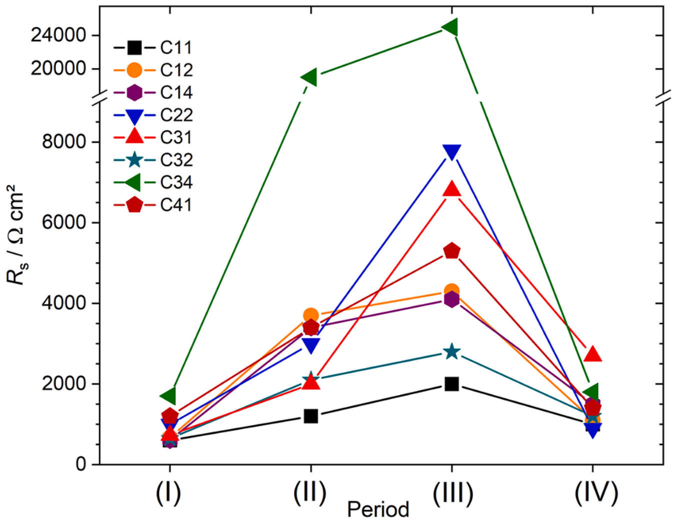

Fig. 6. Evolution of soil resistance R_s of coupons C11, C12, C14, C22, C31, C32, C34 and C41 over the four considered periods.

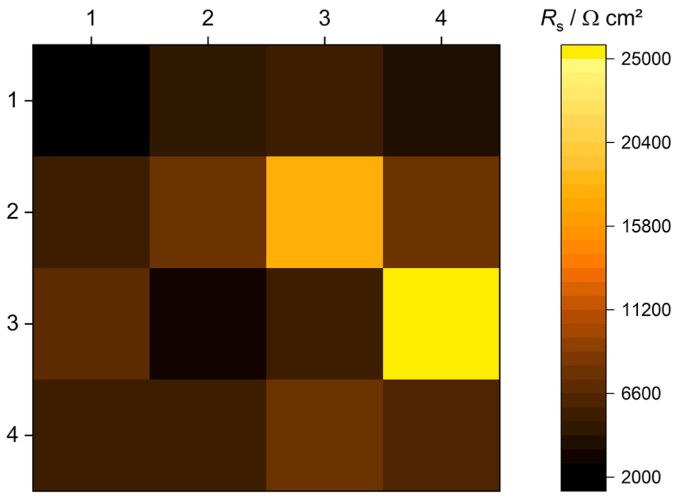

Fig. 7. 2D representation of the average R_s values measured at period (III) for the 16 coupons of the MCE.

remained high because the renewed electrolyte provided a sufficient amount of O_2 that was not consumed, even at the vicinity of the coupons, at the end of period (IV). The highest value of R_s at the end of the experiment was that of coupon C43. The soil was the most aerated and the driest at the vicinity of this coupon.

3.3. X-ray diffraction analysis of the coupons

The results obtained are listed in Table 3 while four representative XRD patterns are displayed in Fig. 8.

The main corrosion product is goethite (α-FeOOH), identified on all coupons (16/16). Another Fe(III) oxyhydroxide, lepidocrocite (γ-FeOOH), was also detected on half of the coupons (8/16), but often as a minor component. Actually, the formation of lepidocrocite from Fe(II)-based compounds requires fast oxidation kinetic, i.e. an important oxygen flow, whereas goethite is rather characteristic of a moderate aeration [20,21]. In various similar previous studies, independently of the type of aerated soil, goethite was identified as the main corrosion product [6,7]. The observed lepidocrocite could therefore partly result from post-excavation oxidation before glycerol was set on the MCE surface, when oxygen (from air) could more easily reach the Fe(II)-based compounds present in the corrosion product layer.

Table 3
Synthesis of the XRD analysis performed on each of the 16 coupons Cij of the MCE. Minor components are mentioned in italics in brackets.

	Ci1	Ci2	Ci3	Ci4
C1j	$FeCO_3$ GR(Cl^-) GR(SO_4^{2-}) GR(CO_3^{2-}) Fe_3O_4 α-FeOOH *(γ-FeOOH)*	Fe_3O_4 α-FeOOH	$FeCO_3$ α-FeOOH *(γ-FeOOH)*	*($FeCO_3$)* Fe_3O_4 α-FeOOH
C2j	Fe_3O_4 α-FeOOH g-FeOOH	$FeCO_3$ GR(CO_3^{2-}) (Fe_3O_4) α-FeOOH	Fe_3O_4 α-FeOOH *(γ-FeOOH)*	Fe_3O_4 α-FeOOH
C3j	$FeCO_3$ Fe_3O_4 α-FeOOH *(γ-FeOOH)*	$FeCO_3$ GR(Cl^-) GR(SO_4^{2-}) (Fe_3O_4) α -FeOOH *(γ -FeOOH)*	$FeCO_3$ Fe_3O_4 α-FeOOH	$FeCO_3$ Fe_3O_4 α-FeOOH
C4j	$FeCO_3$ Fe_3O_4 α-FeOOH γ-FeOOH	$FeCO_3$ Fe_3O_4 α-FeOOH *(γ-FeOOH)*	α-FeOOH	$FeCO_3$ Fe_3O_4 α-FeOOH

Magnetite Fe_3O_4 was identified on 14 of the 16 coupons (i.e., not detected only for C13 and C43). Like goethite and lepidocrocite, it can be obtained by oxidation of Fe(II)-based compounds. For instance, it can be obtained from green rust (GR) compounds when the aeration level is very low [22]. It may also form directly from the metal itself even in anoxic conditions [23].

Siderite ($FeCO_3$) was identified on 11 of the 16 coupons (not detected only for C12, C21, C23, C24 and C43), which may be attributed to the electrolyte used in this study, i.e., a 0.01 M NaCl + 0.01 M $NaHCO_3$ solution. Siderite can then form on the metal surface via the reaction between Fe^{2+} ions that result from corrosion and carbonate species present in the soil electrolyte.

Green rusts were observed on coupons C22, C32 and C11. The last coupon deviated the most from the general trend as it was covered with a particularly compact black corrosion product layer. A fragment of this layer could be scraped from the coupon surface and analyzed separately, with the side corresponding to the steel/fragment interface facing the X-ray beam (Fig. 9). This second X-ray diffraction pattern revealed the presence of siderite and chloride green rust in addition to sulfate green rust and carbonate green rust already identified via the first XRD pattern (Fig. 8). The carbonate green rust GR(CO_3^{2-}) was then identified on coupons C11 and C22, and the chloride green rust GR(Cl^-) on coupons C11 and C32. Like that of siderite, the formation of these compounds can be linked with the composition of the electrolyte used to wet the soil, which contains HCO_3^- and Cl^- ions. In contrast, the formation of the sulfate green rust GR(SO_4^{2-}), identified on coupons C11 and C32, cannot be linked to the electrolyte composition. It is then linked to the soil itself. Actually, sulfate species were present in the peat used to prepare the artificial soil. The specific composition of the corrosion product layers of coupons C11 and C32 can then be attributed to a larger (than the average) amount of peat at the soil/steel interface.

The link between the composition of the corrosion product layer and the local aeration/moisture is thoroughly discussed in Section 4.1.

3.4. Observation and analysis of coupons surface by optical microscopy

Fig. 10 shows OM images of the surfaces of coupons C11, C21, C42 and C34 after removal of the corrosion product layer (as described in Section 2.3). The OM images clearly reveal the localized nature of the corrosion process. The surfaces all show various areas more or less corroded.

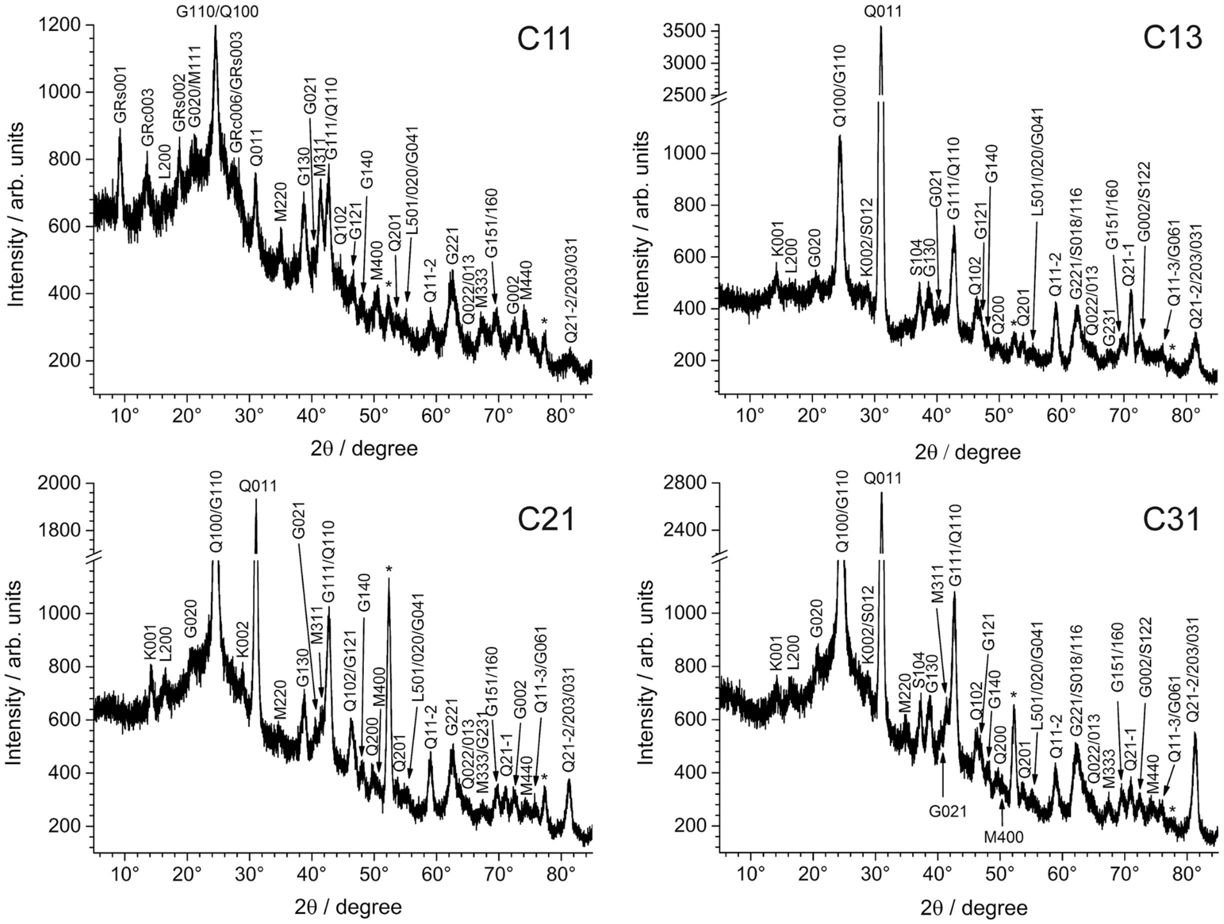

Fig. 8. XRD patterns of coupons C11, C13, C21 and C31. G = goethite, GRc = carbonate green rust, GRs = sulfate green rust, K = kaolinite, L = lepidocrocite, M = magnetite, Q = quartz, and S = siderite. The diffraction lines are denoted with the corresponding Miller index.

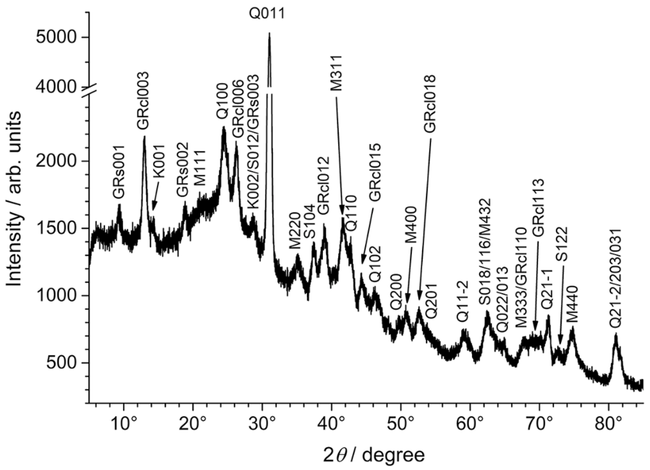

Fig. 9. XRD pattern of a fragment of the corrosion product layer covering coupon C11, analyzed separately. GRcl = chloride green rust, GRs = sulfate green rust, K = kaolinite, M = magnetite, Q = quartz, and S = siderite. The diffraction lines are denoted with the corresponding Miller index.

In all cases, two major types of large zones appear. The bright areas are generally less degraded, while darker areas are more corroded. The first ones can be called WCZ, for weakly corroded zones, and the others LCZ, for large corroded zones. The WCZ probably correspond to metal surface parts that have rapidly become in contact with a rather dry soil. In most cases, the polishing streaks can still be seen. The LCZ correspond to the parts that remained in contact with a wet soil for a longer time. For the sake of clarity, Fig. 11 displays different corrosion depth profiles of coupon C11, obtained with the OM. The first Fig. 11A shows the transition between a LCZ (left) and a WCZ, with a “pit” in the WCZ on the right. The second Fig. 11B mainly shows a WCZ, with the transition on the left and a “pit” on the right. Finally, Fig. 11C is focused on a LZC, with a small part of the adjacent WCZ on the right.

In each kind of zones, the corrosion is not uniform. In the LCZ covered by wet regions of soil, many “pits” can be seen (Fig. 11C). These “pits”, where corrosion was more active, may correspond to the soil pore outlets where the electrolyte came into direct contact with the metal. Between two “pits”, the metal was then in contact with solid particles of the soil. In WCZ covered by drier parts of soil, the weakly degraded surface was rather flat (Fig. 11B). However, a few pits appear here and there (Figs 11A and 11B). These regions could correspond to an area of the metal that remained under a droplet of water.

Table 4 summarizes the average depths and widths of LCZ and pits of WCZ. The depths were measured with respect to the surrounding parts of the 3D-printed mold of the MCE. The average depths in the LCZ vary from 23 μm (C22) to 69 μm (C14). The maximum depth observed is between 40 μm (C22) and 160 μm (C14). The pits in the WCZ do not correspond to a severe degradation, as their average depth is about 10–15 μm, with a maximum that does not exceed 25 μm (C21).

Considering both LCZ depth and WCZ pits depth, C31 can be considered as the least degraded coupon. This result is interesting because the electrochemical measurements indicated its possible role as a cathode, compared to neighboring coupons. However, coupon C32, which had a low potential and may have played the role of an anode, did not undergo a particularly important attack. It can be forwarded that

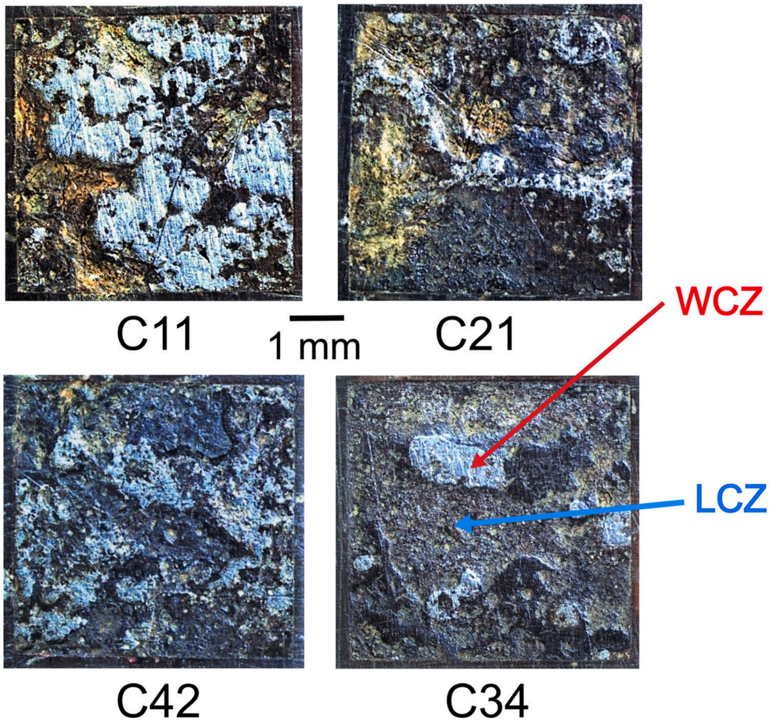

Fig. 10. OM observation of the surface of coupons C11, C21, C42 and C34 after removal of the corrosion products.

C31 acted as cathode with respect to all of its 5 neighboring coupons. Moreover, the morphology of the corrosion process seems to indicate that galvanic couplings associated with differential aeration cells are active essentially over shorter distances than coupons dimensions. This last point is discussed in Section 4.2.

C34 was one of the two coupons with the highest R_s. It may have been located in a zone where the soil quickly dried so that the active area became rapidly very low. This means that the transition period, when wet and dry zones coexisted, was brief. The LCZ degradation, assumed to correspond to the metal surface in contact with the wettest parts of soil for a long time, has therefore taken place over a shorter period, hence, is less important than the average (Table 4).

Considering that the corrosion was effective mainly after cell opening on day 32 which allowed re-aeration near the MCE, i.e., only for 93 days, the average corrosion rates can be estimated from heights H (given in Table 4):

- Average corrosion rate in LCZ: 90 µm yr^{-1} (C22) to 270 µm yr^{-1} (C14).
- Maximum observed in LCZ: 155 µm yr^{-1} (C22) to 630 µm yr^{-1} (C14).
- WCZ pits: maximum equal to 100 µm yr^{-1} (C21).

These corrosion rates are the same order of magnitude as those observed in the same soil wetted with a 0.01 mol L^{-1} NaCl solution [6]. Changing the electrolyte had thus no significant effect in terms of corrosion rates in this case. Various previous works reported important localized corrosion rates [7,12,24]. For instance, average pitting rates up to 450 µm yr^{-1} were measured in Swedish natural sites after three years in soil (muddy clay) [24].

Note that the corrosion rates reported in the present study were determined from local OM measurements and correspond to localized corrosion rates. They vary, considering the whole 4 cm^2 MCE surface, from 90 µm yr^{-1} (average in the less degraded region corresponding to C22) to 630 µm yr^{-1} (most degraded area of C14.) As far as pipelines are concerned, the hazardous corrosion failure is localized corrosion that can lead to leaking.

4. Discussion

4.1. Formation of corrosion products and aeration

According to XRD analysis, the main corrosion process involves siderite, magnetite and goethite. Siderite is a Fe(II) compound and is thus formed first from the Fe^{2+} species produced by the anodic reaction:

$$Fe \rightarrow Fe^{2+} + 2e^- \quad (1)$$

Considering the pH of the soil, i.e., 7.3 ± 0.1, the main carbonate species is HCO_3^-, so that siderite forms according to the following reaction:

$$Fe^{2+} + HCO_3^- \rightarrow FeCO_3 + H^+ \quad (2)$$

The reduction of oxygen is the main cathodic process associated with the anodic reaction:

$$½O_2 + H_2O + 2e^- \rightarrow 2OH^- \quad (3)$$

The overall reaction for siderite formation is then:

$$Fe + ½O_2 + HCO_3^- \rightarrow FeCO_3 + OH^- \quad (4)$$

This reaction produces one OH^- ion per each oxidized Fe atom. Because of the buffering action of the hydrogenocarbonate ions, pH may however not vary due to the formation of a carbonate ion:

$$HCO_3^- + OH^- \rightarrow CO_3^{2-} + H_2O \quad (5)$$

During the first period (I) of the experiment where soil moisture was high (75% sat.), the oxygen flow was low so that siderite oxidation was probably limited and siderite may have accumulated at the metal surface. Magnetite Fe_3O_4 would be the main oxidation product of $FeCO_3$ [21]:

$$3FeCO_3 + 1/2O_2 + 3H_2O \rightarrow Fe_3O_4 + 3HCO_3^- + 3H^+ \quad (6)$$

This oxidation reaction produces 1 H^+ ion per $FeCO_3$ formula, when the formation of siderite has previously produced 1 OH^- ion per $FeCO_3$

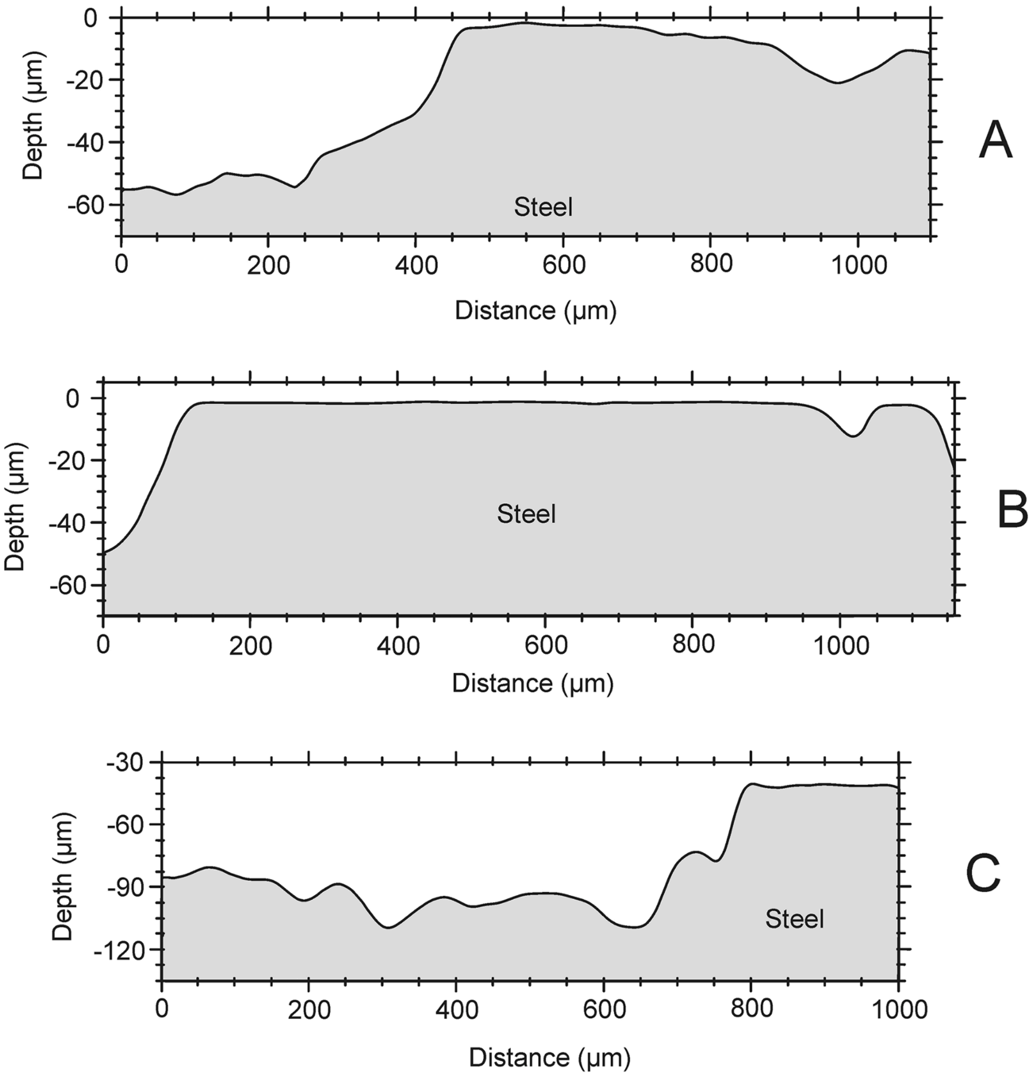

Fig. 11. Typical corrosion depth profiles of coupon C11.

Table 4
Attack depth in the LCZ (*H*), associated error interval (Δ*H*), minimum and maximum observed values; width at the edge (*W*) and depth (*H*) of the observed pits in the WCZ, error interval, minimum and maximum observed values for *W* and *H*.

	Large Corroded Zones (LCZ)			«Pits» of the Weakly Corroded Zones (WCZ)					
	H ± Δ*H* (µm)	*H* mini (µm)	*H* maxi (µm)	*W* ± Δ*W* (µm)	*W* mini (µm)	*W* maxi (µm)	*H* ± Δ*H* (µm)	*H* mini (µm)	*H* maxi (µm)
C11	36 ± 21	10	120	50 ± 10	35	100	10	5	20
C12	65 ± 27	40	115	–	–	–	–	–	–
C13	34 ± 18	4	70	–	–	–	–	–	–
C14	69 ± 43	10	160	40	40	40	5	5	5
C21	39 ± 29	8	100	45 ± 7	35	55	17 ± 6	10	25
C22	23 ± 9	5	40	40	40	40	20	20	20
C23	36 ± 18	15	80	45 ± 7	40	50	7 ± 4	4	10
C24	44 ± 27	10	110	43 ± 3	40	45	8 ± 6	5	15
C31	27 ± 15	5	55	34 ± 11	25	50	11 ± 1	10	12
C32	35 ± 23	10	100	43 ± 6	40	50	9 ± 6	5	15
C33	39 ± 18	20	80	50	50	50	6	6	6
C34	31 ± 11	15	50	30	30	30	10	10	10
C41	38 ± 26	10	120	34 ± 7	25	40	9 ± 3	5	12
C42	65 ± 27	40	115	–	–	–	–	–	–
C43	28 ± 18	10	55	50	50	50	5	5	5
C44	33 ± 16	10	70	–	–	–	–	–	–

formula (Eq. (4)). The carbonate equilibrium would then, conversely to reaction (5), consume the produced H^+ ions:

$$CO_3^{2-} + H^+ \rightarrow HCO_3^- \quad (7)$$

During the second period of the experiment, when the soil dried, the transport of oxygen was facilitated as O_2 could flow in the gas phase inside the pores of the soil. The oxidation of siderite into goethite α-FeOOH was then favored, as observed in aerated carbonated aqueous solutions [25]:

$$FeCO_3 + 1/4O_2 + 3/2H_2O \rightarrow FeOOH + HCO_3^- + H^+ \quad (8)$$

The final composition of the corrosion product layer then depends on the aeration, hence, soil dryness at the vicinity of each coupon. At the very end, the soil is very dry and the corrosion process only takes place on a very small proportion of the coupon surface (i.e., the "wet" area is very small) while siderite is entirely oxidized into goethite. Coupon C43 would illustrate this situation, as goethite was the only identified compound (Table 3). This coupon is also one of those, with C23, C34 and C24, that had the highest R_s values in periods (II) and (III), as seen in Table 2.

Conversely, if the soil stays rather wet, i.e., poorly aerated, the oxidation into magnetite is favored. This situation corresponds to coupons C14, C31, C33, C34, C41, C42 and C44, where siderite and magnetite were identified together with goethite. In agreement, coupons C14, C31, C41, C42 and C44 are characterized by moderate R_s values ($\leq$ 3500 Ω cm^2) in period (II). Other coupons such as coupons C12, C21, C23 and C24 correspond to an intermediate situation where only magnetite and goethite were found. In agreement, R_s values measured for coupons C12, C21 and C24 in period (II) are intermediate between those of the previous coupons and that of coupon C43.

The carbonate green rust, another common corrosion products of steel in carbonate-containing media [25–28], was identified only in two cases, i.e., at the surface of coupons C11 and C22. The corrosion process involving $GR(CO_3^{2-})$ instead of $FeCO_3$ is however very similar:

$$6Fe + 7/2O_2 + 8H_2O + HCO_3^- \rightarrow Fe_4^{II}Fe_2^{III}(OH)_{12}CO_3 \cdot 2H_2O + OH^- \quad (9)$$

This reaction, as for siderite, leads to the production of OH^- ions, while the oxidation reactions of $GR(CO_3^{2-})$ produce a similar amount of H^+ ions. Magnetite is favored at low oxygen flows (rather wet soil), goethite at higher aeration levels [22]:

$$Fe_4^{II}Fe_2^{III}(OH)_{12}CO_3 \cdot 2H_2O + 1/2O_2 \rightarrow 2Fe_3O_4 + HCO_3^- + 7H_2O + H^+ \quad (10)$$

$$Fe_4^{II}Fe_2^{III}(OH)_{12}CO_3 \cdot 2H_2O + O_2 \rightarrow 6FeOOH + HCO_3^- + 4H_2O + H^+ \quad (11)$$

$GR(CO_3^{2-})$ is favored, with respect to siderite, by higher interfacial $[OH^-]/[Fe^{2+}]$ and $[OH^-]/[HCO_3/CO_3^{2-}]$ concentration ratios [29]. Its formation may then be favored locally in zones of the soil where the carbonate species concentration is lower than the average or in cathodic zones of the metal surface where $[OH^-]$ is increased and $[Fe^{2+}]$ is decreased (see reactions 1 and 3), as observed for steel in seawater [30].

The formation of $GR(SO_4^{2-})$ at the surface of coupons C11 and C32, more likely associated with a peat-rich local environment, suggests that the heterogeneity of the soil can also lead to changes in the composition of the corrosion product layer.

Like siderite, GR compounds can only accumulate and remain present at the steel surface if the soil environment remains weakly aerated, i.e., if the soil remains rather wet. Actually, the lowest R_s values were observed, in both periods (II) and (III), for coupon C11, which proved covered by a corrosion product layer containing mainly Fe(II)-based compounds (three GR compounds and siderite). The other coupons where GRs were identified are also coupons with low R_s values in period (II), i.e., C22, or in both periods (II) and (III), i.e., C32.

Thus, the composition of the corrosion product layer proved linked to the average local moisture of the soil and to its local composition. There are however some particular cases. The R_s values measured for coupons C23 and C34 proved abnormally important, with respect to those of other coupons, in both periods (II) and (III). These adjacent coupons share a corner (Fig. 1). It is then possible that a large crack in the soil, running obliquely from C23 to C34, was created at the beginning of the drying process. Filled with air, it would correspond on the metal surface of both coupons to a large electrochemically inactive area, thus leading to large R_s values. The initial R_s values measured in period (I) were moreover the highest for these two coupons (Table 2), which suggests that a smaller crack, or a void filled with air, was already present at the beginning of the experiment.

The corrosion product layer of coupon C13 only contained siderite and goethite. It cannot be excluded, however, that magnetite was present but could not be detected. It is also possible that the soil in contact with this coupon was highly heterogeneous, with aerated areas where $FeCO_3$ was oxidized to goethite and deaerated zones where $FeCO_3$ was not even oxidized to magnetite.

The last case is C33, where various electrochemical measurements were very noisy and had to be discarded (see Table 2 for instance). This case is not discussed further for this reason.

4.2. Morphology of the corrosion

Fig. 12 schematically shows, through a cross section view, the proposed interpretation of the observed corrosion profile, deduced from the various depth profiles obtained on different coupons (see Fig. 11 for coupon C11). It is assumed that the drier regions of the soil, in contact with the WCZ, contain a higher proportion of large particles that facilitated the evaporation of water.

The important corrosion rates measured in the LCZ suggest that galvanic effects took place between aerated areas where O_2 reduction rate can be high and deaerated areas where the anodic reaction may induce a decrease in interfacial pH (reaction 2). Similar conclusions were already reported [8]. Moreover, as observed in soils wetted with moderate NaCl concentrations [12], the metal could be passive in the aerated zones and active in the deaerated zones. Differential aeration cells are thus expected to be active in metal zones located under water droplets [31], i.e., in the WCZ where pits were observed. They are more likely also involved at the boundary between wet/dry soil regions, i.e., the LCZ/WCZ boundary (Fig. 12). The cathodic zones (K) then correspond to the parts of the metal surface in contact with the drier side of the boundary, more aerated. The anodic zones (A) correspond to the parts of the metal surface in contact with a more humid soil, less aerated.

4.3. About the link between OCP and R_s

As demonstrated in previous studies [5–7,32], the evolution of R_s for a metal surface buried in an unsaturated soil is mainly associated with the evolution of the "wet" area and then directly connected with local soil moisture. As discussed in Section 4.1, the evolution of R_s for a given coupon of the MCE can then explain in most cases the composition of the corrosion product layer covering the metal surface. Besides, the changes

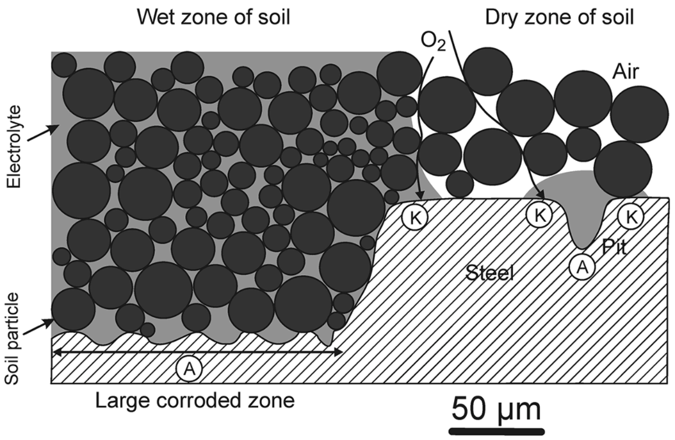

Fig. 12. Schematic representation of the observed corrosion morphology and associated interpretation. A = anodic areas, K = cathodic areas of the steel surface.

in OCP can be connected to the cathodic reaction rate, thus to the local aeration of the soil, which is itself connected to the local soil moisture. Basically, when the soil dries, O_2 transport is facilitated [1,2] and the “wet” area decreases, so that R_s and OCP both increase. This is illustrated in Fig. 13, where the variations of R_s from period (I) to period (IV) are plotted vs. the corresponding variations of OCP for coupons C11, C12, C14, C22, C31 and C43. For each coupon, the progressive drying of the soil, from period (I) to period (III), is associated with a combined increase in both R_s and OCP. However, the amplitude of both variations differs from one coupon to another and the link between the variation of R_s and that of OCP as well.

The smallest variations of both R_s and OCP are observed for coupon C11. This demonstrates that this coupon remained in a rather wet and weakly aerated soil. In contrast, important variations of both R_s and OCP are observed for coupons C22 and C43. In period (III), these coupons were then in a rather dry and aerated soil. However, the evolution was faster for coupon C43, as both R_s and OCP were already high during period (II). This coupon was then most of the time in a strongly aerated soil, which once again explain while only goethite was identified in the corrosion product layer covering coupon C43. Coupons C12 and C14 illustrate the intermediate, or in other words the average, situation. Finally, coupon C31 is a very particular case. During period (II), R_s remained low, while the OCP was already very high. This suggests once again that the surface of this coupon behave as a cathodic site, because the environment was sufficiently wet so that most of the coupon surface remained electrochemically active (low $R_{s,}$ large “wet” area) while O_2 could easily access to this surface (high OCP).

The data obtained during the short (4 days) period (IV) show that the adding of water led in any case to a significant decrease in R_s, which perfectly illustrates the link between R_s and soil moisture. In contrast, the OCP increased slightly or remained constant in most cases (4/6). The renewed electrolyte was saturated with O_2 that fueled the corrosion reaction. This shows that the measurement of both R_s and OCP is necessary to understand the corrosion processes occurring on steel buried in unsaturated soils, especially in “dynamic” conditions where variations of moisture and aeration are taking place.

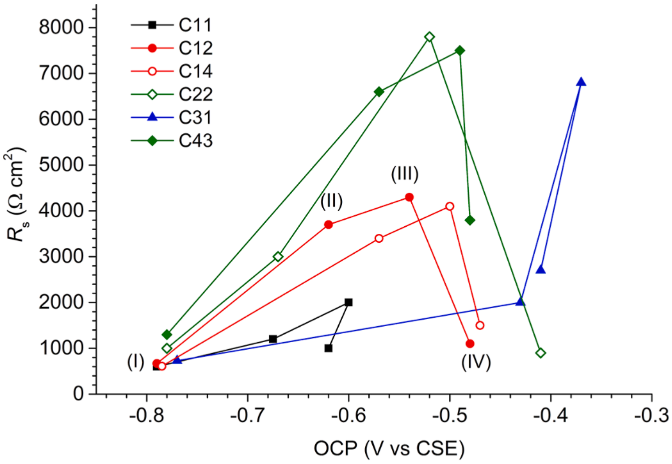

Fig. 13. Evolution of the average soil electrolyte resistance R_s measured at periods (I), (II) (III) and (IV) plotted vs OCP for coupons C11, C12, C14, C22, C31 and C43.

5. Conclusions

The obtained results led to the following information:

- First of all, the multi-coupon electrode (MCE) concept proved relevant to provide crucial information about the corrosion processes taking place on steel surfaces buried in unsaturated soil. The analysis of the electrochemical behavior of each of the 16 coupons of the MCE was fruitfully combined with OM observation of each coupon, and characterization by XRD of each corrosion product layer.
- The variations of composition of the corrosion product layer from one coupon to another mainly resulted from variations of local soil moisture and aeration. These two parameters are qualitatively linked to the soil electrolyte resistance R_s, measured by SIE, and the OCP of the coupons.
- Coupons C11 and C32, characterized by low R_s and OCP values all along the experiment, were covered with specific corrosion products, in particular GR(SO_4^{2-}). A locally high concentration of peat is suspected, as peat was the only source of sulfate present in the system. This shows that local variations of soil composition can induce specific corrosion processes and thus favor corrosion cells.
- The combined measurement of R_s and OCP for each coupon revealed how the drying of the soil could be heterogeneous, as some coupons remained all along the experiment in a rather wet and deaerated soil while others were rapidly in a rather dry and aerated environment. This heterogeneity was also observed at the scale of each coupon. The OM microscopy observations and the corrosion depth profiles revealed the coexistence of large corroded zones (LCZ) and weakly corroded zones (WCZ). The LCZ correspond to parts of the metal surface that remained in contact with a wet soil and suffered corrosion all along the experiment whereas the WCZ correspond to parts of the metal surface that were early in contact with a dry soil.
- The morphology of the corrosion, observed for each coupon, proved localized at a smaller scale than the coupons size (5 mm × 5 mm). Locally important corrosion rates (average 90–270 μm yr^{-1} depending on the coupon, maximum of 630 μm yr^{-1} for coupon C14) were determined, which indicates that differential aeration cells were active, but these cells mainly involved small metal zones on a given coupon, and marginally different coupons. The particular behavior of coupon C31 suggests however that this coupon behave as cathode with respect to surrounding coupons.

Data availability

Data will be made available on request.

CRediT authorship contribution statement

R. Akkouche: Investigation, Data curation, Validation, Writing – original draft. **C. Rémazeilles:** Conceptualization, Methodology, Validation, Supervision, Writing – review & editing. **M. Jeannin:** Conceptualization, Methodology, Validation, Writing – review & editing. **M. Barbalat:** Conceptualization, Methodology, Supervision, Funding acquisition. **Ph. Refait:** Conceptualization, Methodology, Investigation, Data curation, Validation, Supervision, Writing – original draft, Writing – review & editing.

Declaration of Competing Interest

The authors declare that they have no known competing financial interests or personal relationships that could have appeared to influence the work reported in this paper.

Acknowledgments

This work is part of the PhD thesis of Rym Akkouche financially supported by Air Liquide. Many thanks to B. Péraudeau for his technical contribution to the design and manufacturing of electrochemical cell and MCE.

References

[1] L.S. Cole, D. Marney, The science of pipe corrosion: a review of the literature on the corrosion of ferrous metals in soils, Corros. Sci. 56 (2012) 5–16.

[2] C.N. Neale, J.B. Hughes, C.H. Ward, Impacts of unsaturated zone properties on oxygen transport and aquifer reaeration, Ground Water 38 (2000) 784–794.

[3] S.K. Gupta, B.K. Gupta, The critical soil moisture content in the underground corrosion of mild steel, Corros. Sci. 19 (1979) 171–178.

[4] J.N. Murray, P.J. Moran, Influence of moisture on corrosion of pipeline steel in soils using in situ impedance spectroscopy, Corrosion 45 (1989) 34–43.

[5] D. Nguyen Dang, L. Lanarde, M. Jeannin, R. Sabot, Ph. Refait, Influence of soil moisture on the residual corrosion rates of buried carbon steel structures under cathodic protection, Electrochim. Acta 176 (2015) 1410–1419.

[6] R. Akkouche, C. Rémazeilles, M. Jeannin, M. Barbalat, R. Sabot, Ph. Refait, Influence of soil moisture on the corrosion processes of carbon steel in artificial soil: active area and aeration cells, Electrochim. Acta 213 (2016) 698–708.

[7] R. Akkouche, C. Remazeilles, M. Barbalat, R. Sabot, M. Jeannin, Ph. Refait, Electrochemical monitoring of steel/soil interfaces during wet/dry cycles, J. Electrochem. Soc. 164 (2017) C626–C634.

[8] R. Hirata, A. Ooi, E. Tada, A. Nishikata, Influence of the degree of saturation on carbon steel corrosion in soil, Corros. Sci. 189 (2021), 109568.

[9] R.M. Azoor, R.N. Deo, N. Birbilis, J. Kodikara, On the optimum soil moisture for underground corrosion in different soil types, Corros. Sci. 159 (2019), 108116.

[10] E. Levlin, Corrosion of underground structures due to acidification: laboratory investigation, Br. Corros. J. 26 (1991) 63–67.

[11] E. Levlin, Aeration cell corrosion of carbon steel in soil: in situ monitoring cell current and potential, Corros. Sci. 38 (1996) 2083–2090.

[12] N.N. Glazov, S.M. Ukhlovtsev, I.I. Reformatskaya, A.N. Podobaev, I.I. Ashcheulova, Corrosion of carbon steel in soils of varying moisture content, Protect. Met 42 (2006) 601–608.

[13] N.N. Aung, Y.J. Tan, A new method of studying buried steel corrosion and its inhibition using the wire beam electrode, Corros. Sci. 46 (2004) 3057–3067.

[14] Y. Tan, Experimental methods designed for measuring corrosion in highly resistive and inhomogeneous media, Corros. Sci. 53 (2011) 1145–1155.

[15] Ph. Refait, A.M. Grolleau, M. Jeannin, E. François, R. Sabot, Localized corrosion of carbon steel in marine media: galvanic coupling and heterogeneity of the corrosion product layer, Corros. Sci. 111 (2016) 583–595.

[16] Ph. Refait, M. Jeannin, E. François, R. Sabot, A.M. Grolleau, Galvanic corrosion in marine environments: effects associated with the inversion of polarity of Zn /carbon steel couples, Mater. Corros. 70 (2019) 950–961.

[17] NF ISO 11259:1998, Qualité du sol – description simplifiée du sol, AFNOR, La Plaine Saint-Denis, France (1998).

[18] H.C.B. Hansen, Composition, stabilisation, and light absorption of Fe(II)-Fe(III) hydroxycarbonate (green rust), Clay Miner 24 (1989) 663–669.

[19] NF ISO 8407:2010, Corrosion of metals and alloys - removal of corrosion products from corrosion test specimens, AFNOR, La Plaine Saint-Denis, France (2010).

[20] J. Detournay, M. Ghodsi, R. Derie, Kinetic study of the goethite formation by aeration of ferrous hydroxide gels, Ind. Chim. Belge 39 (1974) 695–701.

[21] F. Gilbert, Ph. Refait, F. Lévêque, C. Remazeilles, E. Conforto, Synthesis of goethite from $Fe(OH)_2$ precipitates: influence of Fe(II) concentration and stirring speed, J. Phys. Chem. Solids 69 (2008) 2124–2130.

[22] C. Ruby, M. Abdelmoula, S. Naille, A. Renard, V. Khare, G. Ona-Nguema, G. Morin, J.M.R. Génin, Oxidation modes and thermodynamics of Fe^{II-III} oxyhydroxycarbonate green rust: dissolution-precipitation versus in situ deprotonation, Geochim. Cosmochim. Acta 74 (2010) 953–966.

[23] S. Kesavan, T.A. Mozhi, B.E. Wilde, Potential-pH diagrams for the Fe - Cl^- - H_2O system at 25 to 150°C, Corrosion 45 (1989) 213–215. NACE.

[24] G. Camitz, T.G. Vinka, V. Chaker, J.D. Palmer, Corrosion of steel and metal-coated steel in swedish soils – effects of soil parameters. "Effects of Soil Characteristics On Corrosion", ASTM International, 1989 eds, STP1013-EB.

[25] M. Reffass, R. Sabot, C. Savall, M. Jeannin, J. Creus, Ph. Refait, Localised corrosion of carbon steel in $NaHCO_3$/NaCl electrolytes: role of Fe(II)-containing compounds, Corros. Sci. 48 (2006) 709–726.

[26] P.P. Stampfl, Ein basisches Eisen-II-III-Karbonat in Rost, Corros. Sci. 9 (1969) 185–187.

[27] M. Abdelmoula, Ph. Refait, S.H. Drissi, J.P. Mihé, J.M. Génin, Conversion electron mössbauer spectroscopy and X-ray diffraction studies of the formation of carbonate-containing green rust one by corrosion of metallic iron in $NaHCO_3$ and ($NaHCO_3$ + NaCl) solutions, Corros. Sci. 38 (1996) 623–633.

[28] L. Legrand, S. Savoye, A. Chausse, R. Messina, Study of oxidation products formed on iron in solutions containing bicarbonate/carbonate, Electrochim. Acta 46 (2000) 111–117.

[29] Ph. Refait, J.A. Bourdoiseau, M. Jeannin, D.D. Nguyen, A. Romaine, R. Sabot, Electrochemical formation of carbonated corrosion products on carbon steel in deaerated solutions, Electrochim. Acta 79 (2012) 210–217.

[30] J. Duboscq, R. Sabot, M. Jeannin, Ph. Refait, Localized corrosion of carbon steel in seawater: processes occurring in cathodic zones, Mater. Corros. 70 (2019) 973–984.

[31] J. Jiang, J. Wang, Y.H. Lu, J.Z. Hu, Effect of length of gas/liquid/solid three-phase boundary (TPB) zone on cathodic and corrosion behavior of metals, Electrochim. Acta. 54 (2009) 1426–1435.

[32] M.G.R. Mahlobo, P.A. Olubambi, M. Jeannin, Ph. Refait, Cathodic protection of buried steel structures: processes occurring at the steel/soil interface during wet/dry cycles, Mater. Corros. 71 (2020) 451–463.